Eur. Phys. J. D **21**, 3–12 (2002)
DOI: 10.1140/epjd/e2002-00180-5

THE EUROPEAN PHYSICAL JOURNAL D

Quasi-molecular resonances in muonic charge-exchange reactions

V.I. Savichev and R. Blümel[a]

Department of Physics, Wesleyan University, Middletown, CT 06459-0155, USA

Received 7 January 2002 / Received in final form 15 April 2002

Abstract. We present the first thorough theoretical discussion of non-monotonic structure in the temporal behavior of X-ray fluorescence intensity spectra of muon charge-exchange reactions of the type $p\mu + Z \to p + \mu Z$. Our discussion is based on semiclassical methods; our results are almost entirely analytical. We find that the reported experimental maxima of muon charge-exchange rates are very close to the theoretical limits. We identify a new quantum mechanism, *quantum impedance matching*, which explains observed inelastic transitions close to the Unitarity Limit. We investigate the specific example of the reaction $p\mu\mathrm{O}^{8+}$ in detail using two-center Coulomb adiabatic potential terms. We find that quantum impedance matched higher-order partial-wave resonances yielding muon-transfer rates close to the Unitarity Limit are responsible for the remarkable non-monotonic structure in the X-ray fluorescence spectra.

PACS. 34.60.+z Scattering in highly excited states (e.g., Rydberg states)

1 Introduction

The presence of high-Z elements in the plasma of a thermonuclear fusion reactor is highly undesirable. High-Z elements "poison" the fusion plasma, resulting in reduced fusion power output [1]. The same is true for Muon Catalyzed Fusion where high-Z elements "steal" muons, which then are no longer available to catalyze fusion reactions. Because of the detrimental effect of high-Z elements, it is not surprising that a number of experiments were performed investigating the details of muon charge transfer from the hydrogen isotopes (protium, deuterium) to elements with high $Z \geq 6$ (carbon, nitrogen, oxygen, ...) [2–4]. First theoretical work on muon charge-exchange reactions dates back to the 1960's when Gerstein obtained theoretical estimates of the muon-transfer processes [5], which were later extended by Fiorentini and Torelli [6]. While many experimental results can be explained on the basis of this early theoretical work, some experiments still present open questions and outright puzzles. One of these puzzles concerns the presence of non-monotonic structure in the temporal behavior of the fluorescence intensity of hard X-rays generated by reactions of the type $p\mu + Z \to p + \mu Z$. For some specific values of Z (*e.g.* $Z = 8$, oxygen), it was found experimentally [3] that contrary to expectations the temporal behavior of the fluorescence intensity of the emitted X-rays is not modeled well by a single decaying exponent, but requires two decaying exponents for a proper fit to the data. This is illustrated in Figure 1 which shows a sketch of the experimentally measured temporal behavior of the X-ray fluorescence intensity for $Z = 8$. We see that after an initial build-up phase, the overall temporal behavior of the X-ray fluorescence decays on average, but also shows a conspicuous non-monotonic structure at intermediate times. The purpose of this paper is to reveal the physical origin of the non-monotonic structure illustrated in Figure 1. We accomplish this by capturing the physics of these experiments with a simple two-state model, which we solve using both analytical and numerical methods. Our results, based on this model, agree well with the experimental results both qualitatively and quantitatively.

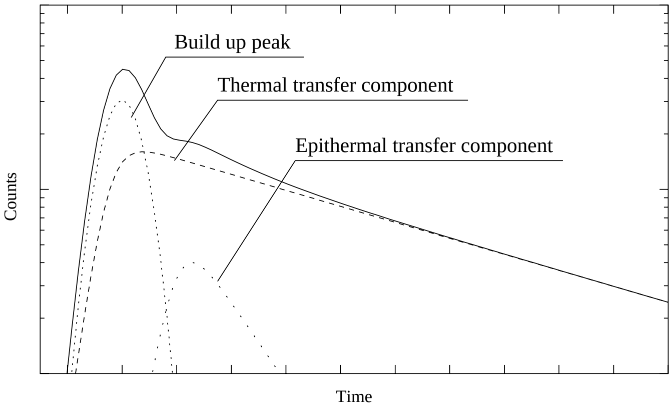

Fig. 1. Sketch of the experimentally measured X-ray fluorescence intensity of muon charge-exchange reactions of the type $(p\mu)Z \to p(\mu Z)$ for $Z = 8$ (oxygen).

The paper is organized in the following way. Since our theory addresses a specific experimental situation, and is directed towards the explanation of actual experimental

---

[a] e-mail: `rblumel@wesleyan.edu`

results, we feel strongly that the reader will benefit from a brief review of the experiments presented in Section 2. In Section 3 we present a qualitative explanation for the observed non-monotonic structure in the X-ray fluorescence intensity. We argue that two ingredients are necessary for a complete explanation of the data. (i) The presence of a resonance or avoided crossing of the adiabatic states of the (μZp) system and (ii) a mechanism that, for specific Z (*e.g.* $Z = 8$), drastically enhances the muon-transfer rates. We identified this mechanism. It is a new quantum mechanism, which involves a quantum matching condition akin to the impedance matching condition well-known in microwave engineering [7]. Thus we call this new mechanism *quantum impedance matching.* Switching from qualitative explanations to quantitative theory, we discuss ingredient (i) in Section 4 from the point of view of the Born-Oppenheimer approximation, which provides the adiabatic states that may exhibit the resonances necessary for ingredient (i). In Section 5 we define an effective two-state model for describing the charge-exchange reaction close to avoided crossings of two adiabatic states. We use this model to compute muon-transfer rates and point out the importance of ingredient (ii), the quantum impedance matching condition, for explaining the observed exceptionally large muon-transfer rates for specific Z values that lead to the non-monotonic structure in the X-ray fluorescence shown in Figure 1. In Section 6 we present our results. In Section 7 we discuss our results, summarize and conclude the paper.

2 Brief review of the experiments

The experiments [2–4] that motivated the investigations reported in this paper were carried out in the following way. A pulsed beam of muons is directed into a chamber containing hydrogen with a small admixture (about 1%) of other high-Z atoms. The pulse duration of the muon beam is very short compared with all other atomic and charge-transfer processes that may occur in this experiment. Immediately following injection of the muons into the hydrogen chamber, both the high-Z elements and the hydrogen atoms compete for muon capture. Muons captured in $(Z\mu)$ excited states decay in a short time interval to the $(Z\mu)$ ground state. The emitted X-rays are recorded by X-ray detectors tuned to particular $(Z\mu)$ $(np \to 1s)$ X-ray emission lines. These X-rays are responsible for the "build-up peak" in Figure 1. Since there is relatively more hydrogen than high-Z elements in the chamber, most of the muons, however, are captured by the hydrogen nuclei, forming highly excited muonic Rydberg states with principal quantum numbers n typically in the range $n \approx 12 \ldots 14$. Within a short time interval the muonic Rydberg states decay to the $(p\mu)$ ground state involving one or a combination of the following three processes (a) radiative decay accompanied by emission of soft X-rays, (b) radiation-less Auger decay involving electron emission by transferring the muon decay energy to surrounding electronic hydrogen atoms/molecules, or (c) radiation-less deexcitation involving collisions followed by direct conversion of the deexcitation energy into kinetic energy of the decaying muonic hydrogen atoms.

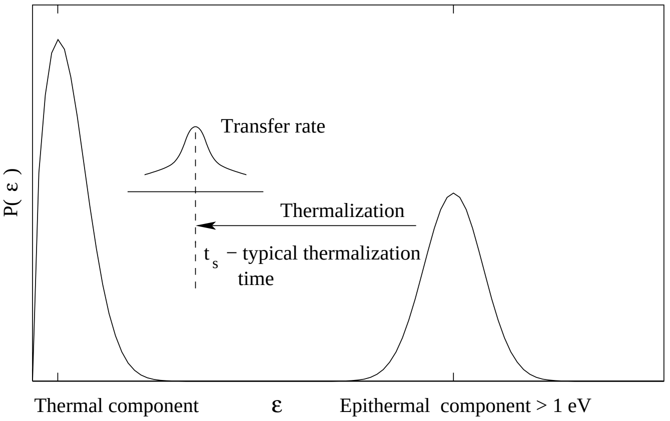

Fig. 2. Sketch of the kinetic energy distribution of $n = 1$ muonic hydrogen atoms immediately after completion of the deexcitation cascade following muon capture. The distribution is bimodal with a "thermal hump" and a "hot component" at kinetic energies $\varepsilon_{\rm kin} \gtrsim 10$ eV. The hot component is due to radiationless processes that transfer (part of) the initial $(p\mu)$ excitation energy directly into the kinetic energy of the $(p\mu)$ muonic hydrogen atom.

The decay mechanism (c) is responsible for the fact that immediately after deexcitation the kinetic energy distribution of the $(p\mu)$ $(n = 1)$ muonic hydrogen atoms is far from thermal equilibrium (see, *e.g.*, Ref. [8]). As sketched schematically in Figure 2, the kinetic energy distribution of the $(p\mu)$ $(n = 1)$ muonic hydrogen atoms shows a clear bimodal distribution with a "thermal hump" at thermal energies ($\varepsilon_{\rm kin} \approx 0.04\,$eV), practically no population in the energy region $0.1\,{\rm eV} \lesssim \varepsilon_{\rm kin} \lesssim 10\,$eV, and another hump at kinetic energies $\varepsilon_{\rm kin} \gtrsim 10\,$eV. The bimodal distribution of the kinetic energy of the muonic hydrogen atoms at the end of the deexcitation process is corroborated by results from experiments with pionic hydrogen atoms, where it was shown that the number of pionic hydrogen atoms with kinetic energy in the region of a few eV and higher can reach up to 50% [8,9]. The high-energy hump in the kinetic energy distribution (see Fig. 2), corresponding to "hot" $(p\mu)$ atoms, will turn out to be crucial for the explanation of the non-monotonic structure in Figure 1. We will return to this point in Section 3.

Once they arrive in the $n = 1$ ground state, the muonic hydrogen atoms may undergo collisions with the nuclei of the high-Z (electronic) atoms present in the chamber. This may result in muonic charge-exchange reactions producing highly excited μZ atomic states, which subsequently decay by emitting hard X-ray photons (X-ray fluorescence). The intensity of the emitted X-rays is recorded as a function of time and results in a spectrum similar to the one shown schematically in Figure 1. To a first approximation the resulting X-ray intensity distribution may be described by a single-exponent decay according to [2]

$$\frac{\mathrm{d}N_{Z\gamma}}{\mathrm{d}t} \sim \exp(-\lambda t), \quad \lambda = \lambda_0 + \frac{\rho}{\rho_0}(c_Z\lambda_Z + c_p\lambda_{pp\mu}), \quad (1)$$

where $N_{Z\gamma}$ is the X-ray intensity of a spectral line observed in the experiment, λ_0 is the muon decay rate, λ_Z is the normalized charge-exchange rate, $\lambda_{pp\mu}$ is the normalized muonic molecule formation rate, c_Z and c_p are the concentrations of the corresponding elements and ρ and ρ_0 are the total atomic density of the investigated mixture and the atomic density of liquid hydrogen, respectively.

Indeed, for instance for the atomic species carbon, neon and sulfur ($Z = 6, 10, 16$, respectively), equation (1) provides a good description of the data. This suggested that charge-exchange reactions, described by equation (1) may provide an excellent tool for monitoring the reaction dynamics of muon catalyzed fusion. But when in one of the first experiments of this type equation (1) was investigated in some more detail with oxygen as the admixed atom, a clear two-exponential structure of the oxygen X-rays was discovered [3] (see Fig. 1 and accompanying discussion in Sect. 1). This means that, while equation (1) may still be useful as a rough first-order monitoring tool, the physics of X-ray production in muonic charge-exchange reactions is more complicated than originally thought, and is a source of interesting physics in its own right. This paper focuses on illuminating and explaining the underlying physical mechanisms that are responsible for the emergence of the second exponent in the temporal behavior of the X-ray intensity.

3 Qualitative explanation of the experimental results

Our explanation of the non-monotonic structure in the X-ray fluorescence data for specific atomic species (see Fig. 1) is based on the "model of two components" [10]. This model suggests that the muon-transfer rate has a maximum in the "epithermal region" $0.1 \leq \varepsilon \leq 1\,\mathrm{eV}$, where ε is the collision energy between a high-Z atom and a muonic hydrogen atom. The purpose of this section is to describe this model in sufficient detail to form an adequate physical background for our theoretical calculations.

As discussed in Section 2, immediately after the muonic hydrogen atoms arrive in the $n = 1$ ground state, their kinetic energies show a bimodal distribution similar to the one sketched in Figure 2. The first hump around $\varepsilon_{\mathrm{kin}} \approx 0.04\,\mathrm{eV}$ corresponds to a thermal distribution of the resulting (μp) atoms, the second hump, at around $10\,\mathrm{eV}$, is the result of radiation-less deexcitation of the muonic hydrogen, where the deexcitation energy is directly converted into kinetic energy of the (μp) atoms (mechanism (c) in Sect. 2). Due to collisions with the cold ambient hydrogen atoms in the chamber, the high-energy hump in Figure 2 is cooling fast and therefore moving to the left, as indicated by the arrow in Figure 2. In case a resonance in the $(p\mu)Z \rightarrow p(\mu Z)$ muon-transfer channel occurs at an energy $\varepsilon_{\mathrm{res}}$ located somewhere between thermal energies and the location of the second hump in Figure 2, the cooling muonic hydrogen atoms, sweeping from right to left, will at one point pass $\varepsilon_{\mathrm{res}}$ and thus have just the right energy for resonant charge transfer to occur.

If resonant muon transfer occurs at some $\varepsilon_{\mathrm{res}}$, we will see its signature as a non-monotonic "bump" in the temporal behavior of the X-ray fluorescence intensity, as indicated in Figure 1. This model also explains why the presence (or absence) of the non-monotonic structure in Figure 1 is so sensitively dependent on Z. This is so because a resonance present for one specific Z may well be completely absent for $Z' \neq Z$. For longer times most of the muonic atoms are thermalized, resulting in an X-ray intensity spectrum which, as shown in Figure 1, can be well described by a single exponent with a decay constant equal to the thermal muon-transfer rate.

Thus the strategy of this paper is clear: we have to look for a resonance mechanism in the $(Z\mu p)$ system which occurs at some energy $\varepsilon_{\mathrm{res}}$, with $\varepsilon_{\mathrm{res}}$ higher than thermal. But due to the very high muon transfer rates measured experimentally, for instance in the case of oxygen, we found that the mere presence of a resonance is not sufficient to explain all aspects of the data. An additional mechanism, we call it *quantum impedance matching*, has to be present. As mentioned above, and discussed in greater detail in Section 5, it is similar to the impedance-matching condition for efficient absorption of microwaves [7]. Thus the further plan of this paper is as follows: in Section 4 we investigate the occurrence of resonances – a necessary condition, as discussed above – in the adiabatic Born-Oppenheimer approach. Then, in Section 5, we investigate the muon-transfer rates within a realistic two-state model and identify the new quantum mechanism.

4 Muonic charge exchange: adiabatic approach

As illustrated in Figure 2, the kinetic energies of the collision partners in the charge exchange reaction $(p\mu)Z \rightarrow p(\mu Z)$ are at most of the order of a few tens of electron volts. As a consequence we are in the regime of very slow atomic collisions. This justifies the application of adiabatic quantum methods, such as the Born-Oppenheimer approach, which we combine with semiclassical techniques in order to explain the nonadiabatic transitions caused by the collisions. We found that the combination of the two methods returns reliable quantitative results.

We work in mesoatomic units where the length scale is given by $a_\mu = a_0/m_\mu$, where a_0 is the Bohr radius and $m_\mu \approx 200\,m_e$ is the muon mass. The collisional mesoatomic processes take place on length scales corresponding to the inter-nuclear distances $R \sim a_\mu$, which are much smaller than the typical size $a_Z \sim a_0/Z$ of the electronic K-shell of an atom with charge Z. To zeroth order we can neglect the influence of the electronic cloud and consider only the effective three-body Coulomb problem $p\mu Z$:

$$\left[-\frac{1}{2M_p}\frac{\mathrm{d}^2}{\mathrm{d}\mathbf{R}_p^2}-\frac{1}{2M_Z}\frac{\mathrm{d}^2}{\mathrm{d}\mathbf{R}_Z^2}-\frac{1}{2m_\mu}\frac{\mathrm{d}^2}{\mathrm{d}\mathbf{r}_\mu^2}+\frac{Z}{|\mathbf{R}_p-\mathbf{R}_Z|}-\frac{1}{|\mathbf{r}_\mu-\mathbf{R}_p|}-\frac{Z}{|\mathbf{r}_\mu-\mathbf{R}_Z|}\right]\Psi=E\Psi. \quad (2)$$

The usual procedure is to separate the center-of-mass motion, introducing Jacobi coordinates [11]. Three possible sets of Jacobi coordinates are illustrated in Figure 3. The set (a) is appropriate in connection with quasi-molecular inelastic transitions:

$$\mathbf{R}=\mathbf{R}_Z-\mathbf{R}_p, \qquad \mathbf{r}=\mathbf{r}_\mu-\frac{M_p\mathbf{R}_p+M_Z\mathbf{R}_Z}{M_p+M_Z},$$
$$m=\frac{M_p+M_Z}{M_p+M_Z+1}, \qquad M=\frac{M_pM_Z}{M_p+M_Z}\cdot \quad (3)$$

In low-energy collisions the inter-nuclear dynamics is much slower than the muon dynamics. We average over the muon motion and consider the nuclear dynamics in an effective potential resulting from averaging. In a consistent quantum mechanical approach the motion in the **r** coordinate is expanded in the complete set of adiabatic states of the two-center Coulomb problem

$$\left[-\frac{1}{2m}\Delta_{\mathbf{r}}-\frac{Z}{|\mathbf{r}-\frac{M_p}{M_p+M_Z}\mathbf{R}|}-\frac{1}{|\mathbf{r}+\frac{M_Z}{M_p+M_Z}\mathbf{R}|}\right]\times\phi_i(\mathbf{r},R)=E_i(R)\phi_i(\mathbf{r},R). \quad (4)$$

This results in a multi-level Born-Oppenheimer (adiabatic) set of coupled equations for the inter-nuclear coordinate R [12]:

$$\left[-\frac{1}{2M}\frac{\mathrm{d}^2}{\mathrm{d}R^2}+\left(E_i(R)+\frac{Z}{R}+\frac{J(J+1)-m^2}{2MR^2}-E\right)\right]\times\chi_i=\sum_j\hat{V}_{ij}\chi_{ij}(R), \quad (5)$$

where the coupling matrix elements $\hat{V}_{ij}=\hat{V}_{ij}^{\mathrm{R}}+\hat{V}_{ij}^{\mathrm{A}}$ are operators composed of a radial and an angular part. Our primary concern are the radial coupling matrix elements given by

$$\hat{V}_{ij}^{\mathrm{R}}=\frac{1}{2M}\left[\left\langle i\left|\frac{\mathrm{d}^2}{\mathrm{d}R^2}\right|j\right\rangle+2\left\langle i\left|\frac{\mathrm{d}}{\mathrm{d}R}\right|j\right\rangle\frac{\mathrm{d}}{\mathrm{d}R}\right]\cdot \quad (6)$$

In an ideal scenario, the matrix elements of the non-adiabatic coupling are bounded and small except for some localized areas of strong coupling. The contribution of the first term in (6) is proportional to $1/M$ and that of the second term is proportional to $1/\sqrt{M}$. As $R\to\infty$ the non-adiabatic coupling dies out.

For $R\to 0$ the adiabatic states correspond to the asymptotic spherical states (N,L,M) of the united atom with charge $Z+1$. For the other limit, $R\to\infty$, each one of the adiabatic states $\phi_i(\mathbf{r},R)$ corresponds to one of the atomic parabolic states localized on either of the nuclei. The adiabatic bases formulated in the three different sets of Jacobi coordinates illustrated in Figure 3 clearly differ in the asymptotic values of their adiabatic energies $E_i(\infty)$. For adiabatic states localized on protium, the choice (a) leads to $E_i(\infty)=-m(1/2n^2)$, whereas choice (b) results in $E_i(\infty)=-m_p(1/2n^2)$, where $m_p=M_p/(M_p+1)$ is the reduced mass of the $p\mu$ atom. Such differences would be unimportant for the case of electronic atoms. For muonic protium, however, $M_p\sim 9$ and the muonic unit of energy is ∼5.5 keV. Therefore the difference between the two ground states is about $1/2M_p\sim 300$ eV. In order to correct this problem, one has to re-sum the whole set of states localized at protium [13], which is equivalent to a transformation between two different sets of Jacobi coordinates. This problem is discussed further in the Appendix.

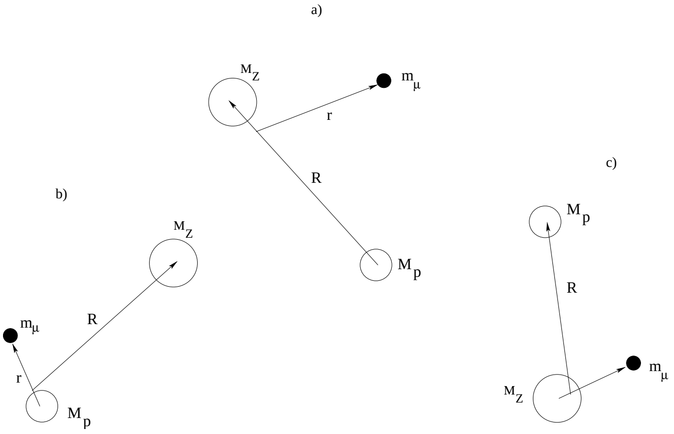

Fig. 3. The complete set of Jacobi coordinates for the three-body problem; (a) is the most relevant set in the quasi-molecular region; (b) and (c) correspond to two possible asymptotic rearrangement channels. Transformation to the correct set of Jacobi coordinates automatically generates the correct reduced mass of the asymptotic complex.

For a direct comparison with experimental results we have to calculate the normalized muon-transfer rates

$$\lambda(\varepsilon)=\rho_0 v\sigma(\varepsilon), \quad (7)$$

where $v=\sqrt{2\varepsilon/M}$ is the collision velocity and ρ_0 is the liquid hydrogen density. The cross section $\sigma(\varepsilon)$ is calculated using the partial wave expansion:

$$\sigma(\varepsilon)=\frac{\pi}{k^2}\sum_{J=0}^{\infty}(2J+1)\left|\delta_{fi}-S_{fi}^{(J)}\right|^2. \quad (8)$$

Here $S_{fi}^{(J)}$ are the matrix elements which have to be extracted from the solutions of the coupled equations (5).

The advantage of the adiabatic approach consists in the fact that at most inter-nuclear distances R, the nonadiabatic coupling matrix elements $\hat{V}_{ij}$ in (5) are small. Strong transitions take place mainly in the narrow localized regions of binary quasicrossings (avoided crossings), such as those sketched in Figure 4. The inverse square

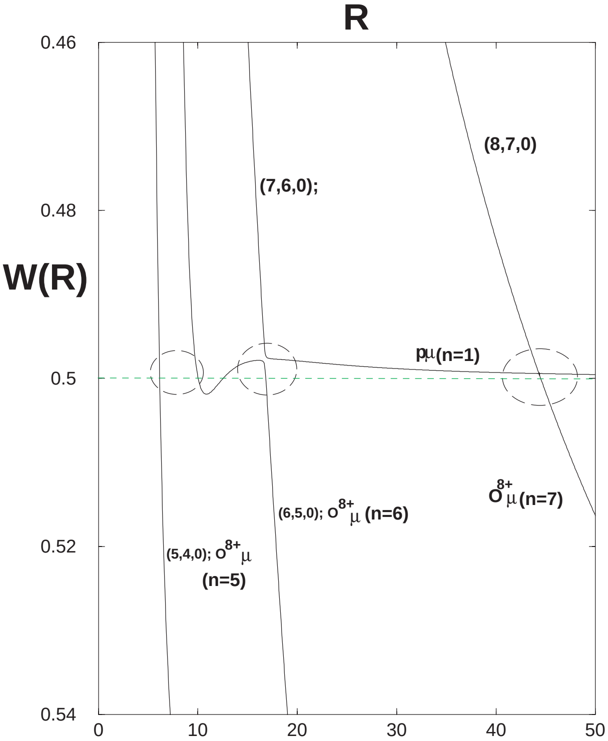

Fig. 4. Adiabatic potential energy curves $W(R)$ as a function of the inter-nuclear distance R for the $p\mu\mathrm{O}^{8+}$ system. The quantum number n is the principal quantum number of the muonic-atomic state in the separated-atom limit. The adiabatic states are labeled by the united atom quantum numbers (N, L, M). The quantum numbers $(8, 7, 0)$ correspond to the $\mu p(1s)$ ground state. The states $(7, 6, 0)$, $(6, 5, 0)$ and $(5, 4, 0)$ correspond to the adiabatic states localized on oxygen for $R \to \infty$. Two very narrow quasi-crossings at large inter-nuclear distances are passed diabatically (highlighted by the two right-most circles). The wide crossing between $(6, 5, 0)$ and $(5, 4, 0)$ at $R \approx 9$ is responsible for enhanced muon transfer.

root of the reduced nuclear mass M plays the role of an effective Planck constant $\hbar_{\text{eff}} \sim 1/\sqrt{M}$, which, if small, guarantees applicability of the semiclassical approach. The construction of the S-matrix may now be reformulated in terms of matching transition matrices [12] with the incoming and outgoing waves of semiclassical motion along the adiabatic potential curves. The well-known Landau-Zener model [14,15] serves as a reference problem for the computation of nonadiabatic transitions in binary quasi-crossings. It is necessary to go beyond this approach if the standard semiclassical approximation is violated by near-barrier quantum effects (tunneling, above barrier reflection) and potential-well motion.

5 Effective two-state model

Formally the number of channels involved in the transitions between a given *in*-channel and some *out*-channel is infinite. Nevertheless some quantitative estimates allow us to reduce the number of physically significant channels to a minimum.

Let us look closely at the quasicrossing region. We can assign a semiclassical one-passage transition probability:

$$P_{ij} = \exp\left(-2\varDelta_{ij}\right). \tag{9}$$

The two-passage transition probability is then given by the expression

$$w_{ij} \sim 2P_{ij}(1 - P_{ij}). \tag{10}$$

This expression for w_{ij} is only a rough estimate. In particular it does not account for the phases in the in- and out-channels. We will present a more accurate theory below. But (10) is still important since it motivates and justifies our choice of the two-state model. The parameter $\varDelta_{ij}$ in (9) is the so-called Massey parameter. It is generally proportional to the product of the minimal splitting between two adiabatic terms and the transition length, and it is inversely proportional to the average velocity in the transition region

$$\varDelta_{ij} \sim \frac{|E_i - E_j| l}{v} \cdot \tag{11}$$

Putting (10) and (11) together, we conclude that the probability of inelastic transitions is small in both limits of "wide" and "narrow" quasicrossings.

Quasicrossings correspond to the exact crossing of two potential curves E_i and E_j in some complex point (branching point) R_{c} [16]. The Massey parameter is defined *via* a complex integral around R_{c}:

$$\varDelta_{ij} = \left| \mathrm{Im} \left[\int_{R_i^{\mathrm{t}}}^{R_{\mathrm{c}}} P_i(R) \mathrm{d}R - \int_{R_j^{\mathrm{t}}}^{R_{\mathrm{c}}} P_j(R) \mathrm{d}R \right] \right|, \tag{12}$$

where $R_i^{\mathrm{t}}, R_j^{\mathrm{t}}$ are the classical turning points, and the quantum momentum $P_i(R)$ and the potential curve $W_i(R)$ of the motion along the given adiabatic term are given by the expressions

$$\begin{aligned} P_i(R) &= \sqrt{2M[\varepsilon - W_i(R)]}, \\ W_i(R) &= E_i(R) + \frac{(J + 1/2)^2}{2MR^2} + \frac{Z_1 Z_2}{R} \cdot \end{aligned} \tag{13}$$

The complex crossing point R_{c} corresponds to a first-order pole-singularity in the non-adiabatic coupling matrix element

$$\left\langle n \left| \frac{\mathrm{d}}{\mathrm{d}R} \right| m \right\rangle \approx \frac{1}{4\mathrm{i}} \frac{1}{R - R_{\mathrm{c}}} \cdot \tag{14}$$

The point R_{c} is an example of the localized positions at which the nonadiabatic coupling matrix elements (6) become large. They will yield important contributions in the numerical integration along the real axis R.

We use the Langer correction in the centrifugal term (13), well-known in the context of the semiclassical approximation [17]. Let us recall that it guarantees correct behavior of the semiclassical solution at $R \to 0$. Interestingly enough it also automatically guarantees the correct

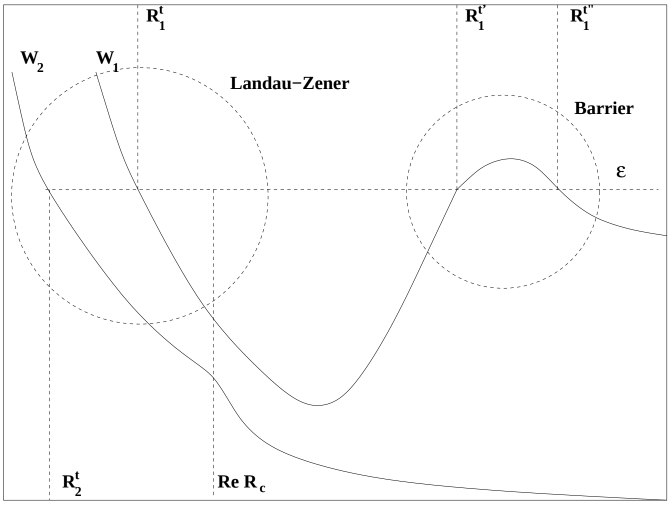

Fig. 5. Illustration of the effective two-state problem. The adiabatic potentials $W_1(R)$ and $W_2(R)$ correspond to the initial and final states of the resulting muon-transfer reaction, respectively. The semiclassical approximation is valid everywhere except in the vicinity of turning points and quasi-crossings areas. The dashed circle to the left highlights the region of internuclear distances which can be described by a Landau-Zener model which consists of two turning points $R_1^{\mathrm{t}}, R_2^{\mathrm{t}}$ and the region of non-adiabatic transition around $\mathrm{Re}R_{\mathrm{c}}$. The dashed circle to the right highlights the barrier area consisting of two turning points $R_1^{\mathrm{t}'}, R_1^{\mathrm{t}''}$ at given collision energy ε.

low-energy behavior at $\varepsilon \to 0$ in the potential with polarization tail $-\alpha/R^4$ [18]. We can further rewrite (12) in the form

$$\Delta_{ij} = \left| \mathrm{Im} \int_{R_{\mathrm{t}}}^{R_{\mathrm{c}}} \frac{E_j(R) - E_i(R)}{v(R)} \mathrm{d}R \right|, \tag{15}$$

where $R_{\mathrm{t}} = \max(R_i^{\mathrm{t}}, R_j^{\mathrm{t}})$ and $v(R) = [v_i(R) + v_j(R)]/2$, $v_i(R) = P_i(R)/M$.

Thus, considering non-adiabatic coupling of the given state, we can drop all but the quasicrossings with $\Delta_{ij} \sim 1$. In the specific case of the $p\mu\mathrm{O}^{8+}$ collisional system, we start to the right in Figure 4 on the initial $p\mu(1s)$ state. The two narrow crossings with the $\mathrm{O}^{8+}\mu(n=7)$, $\mathrm{O}^{8+}\mu(n=6)$ states are traversed diabatically (see [5] for estimates). The charge-exchange process takes place at $R \approx 9$ as a nonadiabatic transition between the states $(6,5,0)$ and $(5,4,0)$. The observed X-ray radiation pattern seems to favour $\mathrm{O}^{8+}\mu(n=5)$ as the main charge-exchange channel [19].

To lowest approximation we restrict ourselves to considering the resulting two-state problem depicted in Figure 5. The required 2×2 S-matrix can be written in closed analytical form using the semiclassical approximation [12]. To do so, we have to match the semiclassical waves coming from the area of non-adiabatic transition and near-barrier motion in the incoming channel, denoted in Figure 5. by “Landau-Zener” and “Barrier”, respectively. The non-adiabatic transition together with the right turning point $R_1^{\mathrm{t}'}$ are characterized by the following S-matrix:

$$S^{\mathrm{LZ}} = \begin{pmatrix} \sqrt{1-P_{\mathrm{LZ}}}\mathrm{e}^{\mathrm{i}2\phi_1} & \mathrm{i}\sqrt{P_{\mathrm{LZ}}}\mathrm{e}^{\mathrm{i}\phi_1+\mathrm{i}\phi_2} \\ \mathrm{i}\sqrt{P_{\mathrm{LZ}}}\mathrm{e}^{\mathrm{i}\phi_1+\mathrm{i}\phi_2} & \sqrt{1-P_{\mathrm{LZ}}}\mathrm{e}^{\mathrm{i}2\phi_2} \end{pmatrix}, \tag{16}$$

where the parameters are given by

$$\begin{aligned} P_{\mathrm{LZ}} &= 4P(1-P)\sin^2\phi_{12}, \\ P &= \mathrm{e}^{-2\Delta_{12}}, \quad \Delta_{12} = \left| \mathrm{Im} \int_{R_1^{\mathrm{t}}}^{R_{\mathrm{c}}} \frac{E_2(R) - E_1(R)}{v(R)} \mathrm{d}R \right|, \\ \phi_1 &= \int_{R_1^{\mathrm{t}}}^{R_{\mathrm{c}}} P_1(R)\mathrm{d}R + \pi/4 - \phi_{\mathrm{LZ}} \\ &\quad - 1/2 \arctan\left[\frac{P_{\mathrm{LZ}}\sin 2\phi_{12}}{1 - 2P_{\mathrm{LZ}}\sin^2\phi_{12}}\right], \\ \phi_2 &= \int_{R_2^{\mathrm{t}}}^{R_{\mathrm{c}}} P_2(R)\mathrm{d}R + \pi/4 + \phi_{\mathrm{LZ}} \\ &\quad + 1/2 \arctan\left[\frac{P_{\mathrm{LZ}}\sin 2\phi_{12}}{1 - 2P_{\mathrm{LZ}}\sin^2\phi_{12}}\right], \\ \phi_{12} &= \mathrm{Re}\left[\int_{R_1^{\mathrm{t}}}^{R_{\mathrm{c}}} P_1(R)\mathrm{d}R - \int_{R_2^{\mathrm{t}}}^{R_{\mathrm{c}}} P_2(R)\mathrm{d}R\right] - \phi_{\mathrm{LZ}}, \\ \phi_{\mathrm{LZ}} &= \pi/4 + (\Delta_{12}/\pi)\ln(\Delta_{12}/\pi) \\ &\quad - \Delta_{12}/\pi - \arg[\Gamma(1 + \mathrm{i}\Delta_{12}/\pi)]. \end{aligned} \tag{17}$$

For the above-barrier case we have to take the top of the barrier as the right turning point. The matrix T connects the incoming semiclassical waves towards the barrier with the outgoing waves and is given by

$$T = \begin{pmatrix} r & t \\ t & r \end{pmatrix}, \tag{18}$$

where the complex reflection and transmission coefficients are given by the relations

$$\begin{aligned} r &= -\mathrm{i}\mathrm{e}^{-\mathrm{i}\phi_{\mathrm{t}}(\delta)}/\sqrt{1 + \mathrm{e}^{2\pi\delta}}, \\ t &= \mathrm{e}^{-\mathrm{i}\phi_{\mathrm{t}}(\delta)}/\sqrt{1 + \mathrm{e}^{-2\pi\delta}}, \\ \delta &= -\frac{1}{\pi}\left| \int_{R_1^{\mathrm{t}'}}^{R_1^{\mathrm{t}''}} P_1(R)\mathrm{d}R \right|, \\ \phi_{\mathrm{t}}(\delta) &= \arg[\Gamma(1/2 + \mathrm{i}\delta)] - \delta\ln|\delta| + \delta. \end{aligned} \tag{19}$$

The expressions are modified for the above-barrier case in the following way: δ becomes positive and has to be calculated between the two complex turning points emerging from the top of the barrier $P_1(R_+^{\mathrm{t}}) = P_1(R_-^{\mathrm{t}}) = 0$; $\phi_{\mathrm{t}}(\delta) = -\phi_{\mathrm{t}}(-\delta)$. The combined reduced scattering matrix s is represented by the expression

$$s = \frac{1}{1 + rS_{11}^{\mathrm{LZ}}} \begin{pmatrix} (S_{11}^{\mathrm{LZ}} + r^*)t/t^* & S_{12}^{\mathrm{LZ}}t \\ S_{21}^{\mathrm{LZ}}t & S_{22}^{\mathrm{LZ}} + r\det S^{\mathrm{LZ}} \end{pmatrix}. \tag{20}$$

The complete S-matrix is augmented by the semiclassical evolution phases to the right of the turning point $R_1^{\mathrm{t}''}$

$$S_{ij} = s_{ij}\mathrm{e}^{\mathrm{i}\int_{R_1^{\mathrm{t}''}}^{R}(P_i(R)-P_i(\infty))\mathrm{d}R + \mathrm{i}\int_{R_1^{\mathrm{t}''}}^{R}(P_j(R)-P_j(\infty))\mathrm{d}R - \mathrm{i}\pi J}. \tag{21}$$

Now that we have all the ingredients in place, we can apply it to the problem of muon charge exchange. The process is described according to equation (8) by the $|S_{21}|^2$ matrix element which can be represented in the following form

$$\begin{aligned}
&|S_{21}|^2 = \\
&\frac{P_{\rm t}P_{\rm LZ}}{(\sqrt{1+P_{\rm t}}-\sqrt{1-P_{\rm LZ}})^2+4\sqrt{(1+P_{\rm t})}\sqrt{1-P_{\rm LZ}}\cos^2\Omega},\\
&\Omega=\int_{R_1^{\rm t}}^{R_1^{\rm t'}}P_1(R){\rm d}R-\phi_{\rm LZ}\\
&\quad -1/2\arctan\left[\frac{P_{\rm LZ}\sin 2\phi_{12}}{1-2P_{\rm LZ}\sin^2\phi_{12}}\right]-\phi_{\rm t}/2,\\
&P_{\rm t}={\rm e}^{2\pi\delta}. \qquad (22)
\end{aligned}$$

Let us look for the resonance conditions. Since the denominator is the sum of two positive terms, the condition $\cos\Omega=0$ will maximize the reaction outcome regardless of the values of $P_{\rm t}$ and $P_{\rm LZ}$. Taking (22) into account we conclude that the relation

$$\Omega=\pi(\nu+1/2) \qquad (23)$$

with integer ν corresponds to some Bohr-Sommerfeld quantization condition in the potential well with the corrections coming from the barrier motion and non-adiabatic transition. It is useful to see how the condition changes in different circumstances. Well below the barrier we have $\delta\leq -1, \phi_{\rm t}(\delta)\approx 0$. The two different limits,

$$\begin{aligned}
&\Omega\approx\int_{R_1^{\rm t}}^{R_1^{\rm t'}}P_1(R){\rm d}R=\pi(\nu+1/2), \qquad P_{\rm LZ}\ll 1,\\
&\Omega\approx\int_{R_2^{\rm t}}^{R_{\rm c}}P_2(R){\rm d}R+\int_{R_{\rm c}}^{R_1^{\rm t'}}P_1(R){\rm d}R\\
&\quad=\pi(\nu+1/2), \qquad P_{\rm LZ}\approx 1, \qquad (24)
\end{aligned}$$

correspond to the quantization in nearly adiabatic and nearly diabatic conditions, respectively. The result is that the actual position of the resonance can differ significantly from the single-potential estimate.

So far we did not discriminate between below- and above-barrier situations. Consider now in more detail low-energy sub-barrier motion when the tunneling probability $P_{\rm t}\ll 1$ is exponentially small. We note that a centrifugal barrier does exist in our approach, even for $J=0$, which reproduces the correct behavior for low-energy quantum mechanical scattering.

Let us expand (22) close to some resonance energy defined by (23). To lowest approximation it is enough to take into account the energy dependence of the phase Ω only. As the limiting cases in (24) suggest, the energy derivative of the phase Ω is proportional to some effective classical period $T_{\rm cl}$ of oscillation in the combined potential well ${\rm d}\Omega/{\rm d}E\approx T_{\rm cl}/2$ and hence $4\cos^2\Omega\approx T_{\rm cl}^2(\varepsilon-\varepsilon_{\rm r})^2$. If we also assume $P_{\rm LZ}<1$ and expand the square roots in (22) to leading order, we get

$$|S_{21}|^2=\frac{(P_{\rm t}f_{\rm cl})(P_{\rm LZ}f_{\rm cl})}{(\varepsilon-\varepsilon_{\rm r})^2+(P_{\rm t}f_{\rm cl}+P_{\rm LZ}f_{\rm cl})^2/4}, \qquad (25)$$

where $f_{\rm cl}=1/T_{\rm cl}$. The quantities $P_{\rm t}f_{\rm cl}$ and $P_{\rm LZ}f_{\rm cl}$ are obviously the probability rates for tunneling or non-adiabatic transitions. The maximum reached at $\varepsilon=\varepsilon_{\rm r}$ depends on the rate-ratios

$$|S_{21}|^2=\begin{cases}P_{\rm LZ}/P_{\rm t}, & \text{for} \quad P_{\rm LZ}/P_{\rm t}\ll 1,\\ P_{\rm t}/P_{\rm LZ}, & \text{for} \quad P_{\rm t}/P_{\rm LZ}\ll 1,\\ 1, & \text{for} \quad P_{\rm LZ}=P_{\rm t}.\end{cases} \qquad (26)$$

The third case deserves special attention. Due to the unitarity of the S-matrix, we get immediately $|S_{11}|$, $|S_{22}|\approx 0$, and the S-matrix acquires the form

$$S={\rm e}^{{\rm i}\phi}\begin{pmatrix}0 & 1\\ 1 & 0\end{pmatrix}. \qquad (27)$$

This means that the resulting charge-exchange reaction rate reaches its absolute maximum, or its Unitarity Limit, for the given partial wave. This mechanism reminds us strongly of the impedance matching condition in microwave engineering [7], where in our case the Landau-Zener probability $P_{\rm LZ}$ takes the place of the microwave absorption probability in the corresponding microwave problem. Therefore we call this effect *quantum impedance matching condition.*

6 Results

To illustrate the theory let us now consider the $p\mu{\rm O}^{8+}$ system in more detail. We will focus on the experiments at room temperature which corresponds to a kinetic energy of about 0.04 eV. As already mentioned, the hot component of the (μp) atoms may extend up to several tens of eV. The Monte-Carlo simulations carried out in [19] show, however, that deexcitation of the energy tail above 1 eV proceeds too fast to be observable within the present experimental setup [2–4]. Hence we will concentrate on the energy dependence below 1 eV. As shown by the tunneling probability plots in Figure 6, the first four partial waves, $J=0,1,2,3$, will be enough to describe charge-exchange cross-sections in this energy region. The high rates $\lambda_{\rm th}=8.5\times 10^{10}\,{\rm s}^{-1}$ and $\lambda_{\rm eth}=3.9\times 10^{11}\,{\rm s}^{-1}$ for thermal and epithermal components, respectively, reported in [19], can be compared with the Unitarity Limit imposed by the s-wave contribution (see Fig. 7). From this we conclude that epithermal resonances must be caused by the contributions of the higher partial waves. Our numerical computations show that the resonances are sensitive enough to the details of the adiabatic potentials to be able to explain the presence or absence of the non-monotonic structure in the X-ray spectrum of Figure 1 for different Z values.

The sensitivity is especially pronounced in the d-wave component, for which the phase $\Omega\approx\pi/2$ at $\varepsilon<0.5\,{\rm eV}$. We found that a clear resonance picture appears when we take electron screening and the muon mass effect (see Appendix) into account, where the electron screening is modeled by the polarization tail $-(9/4)(Z(R)^2/R^4)$ with

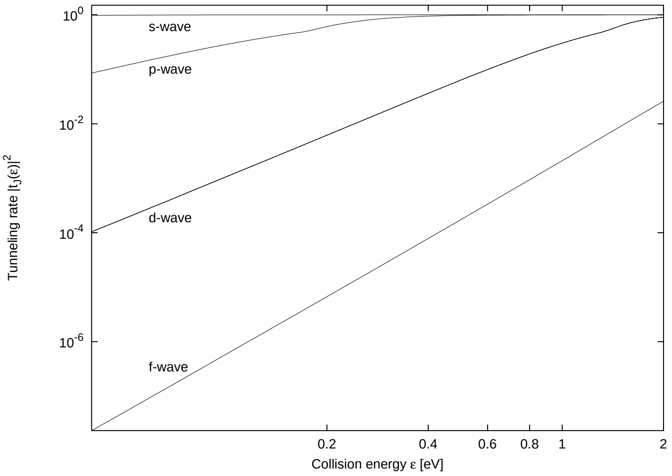

Fig. 6. Tunneling rates $|t_J(\varepsilon)|^2$, including both above and below barrier cases, for partial waves $J = 0, ..., 3$ *versus* collision energy $\varepsilon = 0 \ldots 2\,\mathrm{eV}$. The rates are calculated according to equation (19) with proper modifications for the energies above the barrier.

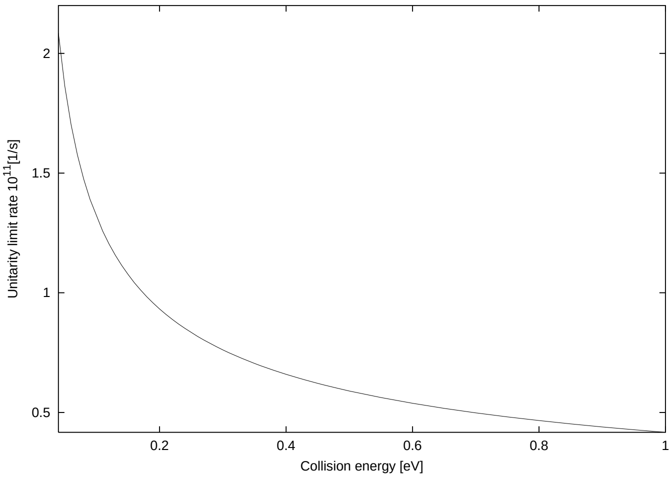

Fig. 7. The s-wave unitarity limit $\rho_0 v\pi/k^2$ for the normalized muon-transfer rate (7).

R-dependent effective charge $Z(R)$. Our final result for the low-energy charge-exchange rate is shown as the full line in Figure 8. The calculations clearly show that below 0.1 eV the rate is dominated by the s-wave contribution. Furthermore, the calculations show that the resonance peak is clearly associated with a d-wave resonance, which is very close to the Unitarity Limit. Our theoretical result (full line in Fig. 8) can be compared with the muon-transfer rates used in state-of-the-art Monte-Carlo calculations [19] (dashed line in Fig. 8). We see that qualitatively, and to some extent even quantitatively, the two rates compare very well. It should be noted, however, that the square-shaped muon-transfer rates used in the Monte-Carlo calculations are not derived microscopically. The shape of these muon-transfer rates is an ad-hoc assumption whose location, height and width are optimized such that Monte-Carlo calculations reproduce the observed temporal behavior of the measured X-ray spectra.

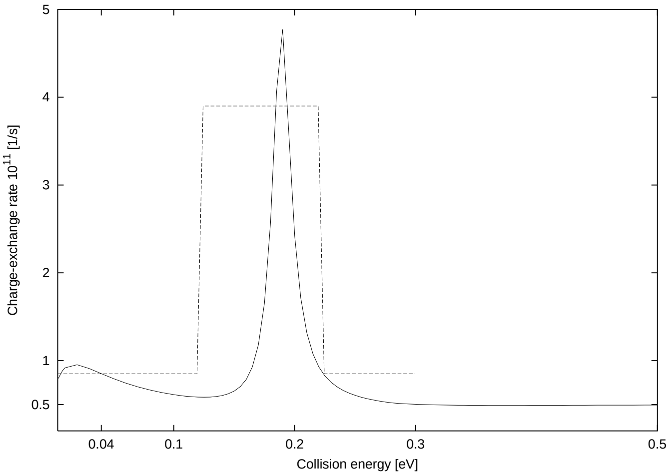

Fig. 8. Full line: low-energy muon-transfer rate $p\mu(1s) + \mathrm{O}^{8+} \to p{+}\mathrm{O}^{8+}\mu(n=5)$ *versus* collision energy $\varepsilon = 0 \ldots 0.5\,\mathrm{eV}$. The muon-transfer rate (7) is calculated in the effective two-level approximation using the first four partial waves $J = 0, ..., 3$ in (8). Dashed line: two-component schematic model of piecewise constant muon-transfer rates as used in Monte-Carlo simulations [19]. The parameters of the schematic model were optimized [19] to fit the experimentally measured temporal behavior of the X-ray fluorescence spectrum.

Let us look at the thermal (i) and epi-thermal (ii) energy regions in detail. (i) A thermal muon-transfer rate of $\lambda_{\mathrm{th}} = 8.5 \times 10^{10}\,\mathrm{s}^{-1}$ can be unambiguously extracted from the long-time tail of the measured temporal X-ray spectrum. We compare it with the thermally weighted energy dependent muon-transfer rate

$$\lambda_{\mathrm{th}} = \int_0^\infty \lambda(\varepsilon) \sqrt{\frac{\varepsilon}{\pi(kT)^3}} \exp(-\varepsilon/kT)\,\mathrm{d}\varepsilon. \qquad (28)$$

Using $\lambda(\varepsilon)$ as defined in (7) and shown explicitly as the full line in Figure 8, we obtain $8.4 \times 10^{10}\,\mathrm{s}^{-1}$. This compares very favorably with the experimental result. (ii) Since, as discussed above, our microscopically computed muon-transfer rates (full line in Fig. 8) are close to the Monte-Carlo muon-transfer rates (dashed line in Fig. 8) we expect that using our muon-transfer rates in state-of-the-art Monte-Carlo calculations, temporal X-ray spectra close to the experimental results will be produced.

7 Discussion, summary and conclusion

Following the experimental discovery of an unexpected second exponent in the time-resolved X-ray spectra in the muonic charge-exchange reaction $(\mu p)\mathrm{O} \to (\mu\mathrm{O})p + \mathrm{X}$, theoretical models were devised to explain this puzzling effect [10]. Although very helpful in shaping our intuition about the effect and focusing the discussion, because of the lack of an underlying physical mechanism, these models were only partially successful. This situation changed when about five years ago one of the present authors

(V.I.S.) suggested a direct physical mechanism for the explanation of the second decay exponent: the presence of quasi-molecular resonances in the $(p\mu)$-oxygen charge-exchange reaction (see introduction of Ref. [20]). Subsequently the presence of resonances in the elastic channel was indeed confirmed [20]. It was argued that these resonances should also manifest themselves in the inelastic channels leading to an explanation of the second exponent. Although highly plausible, the authors of [20] did not present a proof for this conjecture. The missing proof is provided in this paper. Based on semiclassical techniques combined with numerical calculations we obtain very convincing agreement with experimental results. We noticed, however, that the resonances alone do not account for the agreement. An additional quantum mechanism is necessary to explain the experimental results. This mechanism, discussed in detail in Section 5, reminds us of the impedance matching condition in microwave engineering. In our case a large effect is observed only if the tunneling rate and the absorption rate are matched.

In summary, based on a detailed semiclassical study of the muonic hydrogen–oxygen scattering process, combined with the application of a new quantum effect, which we call *quantum impedance matching*, we arrived at a theoretical explanation of the presence of a second exponent in the time-resolved X-ray spectra. We obtain agreement with the experimental results both on the qualitative and quantitative levels.

V.I.S. would like to thank Hubert Schneuwly and Andreas Werthmüller for stimulating discussions. This research was supported by the National Science Foundation under Grant No. 9984075.

Appendix: Muonic mass effect

In Section 4 we mentioned already that the correct muonic atomic masses present a problem. It manifests itself, in particular, in the fact that the matrix of the non-adiabatic couplings does not go to zero for $R \to \infty$. We can use it, however, to effectively improve our computations and include reduced atomic-mass effects without tedious resumation. Consider the matrix element $\langle n|\mathrm{d}^2/\mathrm{d}R^2|n\rangle$ for $R \to \infty$. If the adiabatic state $\phi_n(\mathbf{r}, R)$ corresponds to one of the protium parabolic states (n, n_1, n_2, m), it will acquire the form $\phi(\mathbf{r} - M_\mathrm{O}/(M_\mathrm{O} + M_p)\mathbf{R})$ at $R \to \infty$. Taking into account the relations $M_\mathrm{O} \gg M_p \gg 1$, we estimate the contribution of the matrix element as:

$$\frac{1}{2M}\left\langle n\left|\frac{\mathrm{d}^2}{\mathrm{d}R^2}\right|n\right\rangle \approx -\frac{1}{M_p}\frac{1}{2n^2}\,. \tag{29}$$

Combined with the adiabatic energy asymptotics $-1/2n^2$ it will result in the correct reduced atomic energy to first order in $1/M_p$: $-[M_p/(M_p+1)]/2n^2 \approx -(1-1/M_p)/2n^2$. This simple solution will not produce the right order of magnitude correction for oxygen states but the reduced-mass defect for them is an order of magnitude smaller. In addition using the completeness relations, it is instructive to show that the matrix element $\langle n|\mathrm{d}^2/\mathrm{d}R^2|n\rangle$ contains contributions from all other states coupled to the given state n:

$$\left\langle n\left|\frac{\mathrm{d}^2}{\mathrm{d}R^2}\right|n\right\rangle = \sum_j \left\langle n\left|\frac{\mathrm{d}}{\mathrm{d}R}\right|j\right\rangle \left\langle j\left|\frac{\mathrm{d}}{\mathrm{d}R}\right|n\right\rangle. \tag{30}$$

We suggest now the following procedure tackling the $p\mu(1s)$ state in the effective two-state model. Keeping the constant mass correction term (29) for the incoming $p\mu(1s)$-state will result in changing the reference energy by $1/(2M_p) \approx 300\,\mathrm{eV}$, $\varepsilon = E - (E_{1s}(\infty) + 1/(2M_p))$. Nothing will change for the $p\mu(1s)$-related state itself. All the oxygen related states lying below will acquire an additional energy gap of $1/(2M_p)$ in comparison to the $p\mu(1s)$-related adiabatic state. Close to the transition point we have to skip the constant reduced-mass correction term, as it becomes a small correction in the sum (30), where the main contribution comes from the second-order pole which is related to the complex crossing transition point R_c. The presence of this main singularity, however, is already taken fully into account in the Landau-Zener model and hence in the semiclassical expressions (15, 17, 20). Instead of using some arbitrary switching multiplier, we can apply expressions in the spirit of (15) keeping the constant mass-correction term. We have to slightly modify the calculation of the required phases. For ϕ_{12} in (17) we use the following expression:

$$\phi_{12} = \mathrm{Re}\int_{R_{\mathrm{t}_1}}^{R_\mathrm{c}} \frac{E_2(R) - E_1(R)}{v(R)}\mathrm{d}R - \int_{R_2^\mathrm{t}}^{R_1^\mathrm{t}} P_2(R)\mathrm{d}R, \tag{31}$$

which is fully equivalent to the original one, but also preserves the logical consistency with the constant mass-correction term included.

References

1. *Encyclopedia of Physics*, edited by R.G. Lerner, G.L. Trigg, 2nd edn. (VCH Publishers, New York, 1991)
2. R. Jacot-Guillarmod, F. Bienz, M. Boschung, C. Piller, L.A. Schaller, L. Schellenberg, H. Schneuwly, W. Reichart, G. Torelli, Phys. Rev. A **38**, 6151 (1988)
3. H. Schneuwly, R. Jacot-Guillarmod, F. Mulhauser, P. Oberson, G. Piller, L. Schellenberg, Phys. Lett. A **132**, 335 (1988)
4. L. Schellenberg, A. Adamczak, R. Jacot-Guillarmod, F. Mulhauser, C. Piller, L.A. Schaller, H. Schneuwly, Y.-A. Thalmann, S. Tresch, A. Werthmüller, Hyperf. Interact. **101/102**, 215 (1996)
5. S.S. Gerstein, Sov. Phys. JETP **16**, 501 (1963).
6. G. Fiorentini, G. Torelli, Nuovo Cim. A **36**, 317 (1976)
7. J.D. Jackson, *Classical Electrodynamics*, 2nd edn. (John Wiley & Sons, New York, 1975)
8. A. Badertscher, M. Daum, P.F.A. Goudsmit, M. Janousch, P.-R. Kettle, J. Koglin, V.E. Markushin, J. Schottmüller, Z.G. Zhao, Europhys. Lett. **54**, 313 (2001)

9. J.F. Crawford, M. Daum, R. Frosch, B. Jost, P.R. Kettle, R.M. Marshall, B.K. Wright, K.O.H. Ziock, Phys. Rev. D **43**, 46 (1991)
10. H. Schneuwly, Phys. Lett. A **191**, 416 (1994)
11. L.D. Faddeev, S.P. Merkuriev, *Quantum Scattering Theory for Several Particle Systems* (Kluwer Academic Publishers, Dordrecht, 1993)
12. E.E. Nikitin, S.Ya. Umanskii, *Theory of Slow Atomic Collisions* (Springer, Berlin, 1984)
13. L.I. Ponomarev, L.N. Somov, F. Vukajlovic, J. Phys. B. **14**, 591 (1981)
14. L.D. Landau, Phys. Z. Sowjet. **1**, 88 (1932)
15. C. Zener, Proc. R. Soc. A **137**, 696 (1932)
16. E.A. Solov'ev, Sov. Phys. Usp. **32**, 228 (1989)
17. R.E. Langer, Phys. Rev. **51**, 669 (1937)
18. A.M. Perelomov, Ya.B. Zel'dovich, *Quantum Mechanics: Selected Topics* (World Scientific, Singapore, 1998)
19. A. Werthmüller, A. Adamczak, R. Jacot-Guillarmod, F. Mulhauser, L.A. Schaller, L. Schellenberg, H. Schneuwly, Y.-A. Thalmann, S. Tresch, Hyperf. Interact. **116**, 1 (1998)
20. A. Kravtsov, A. Mikhailov, N. Popov, Phys. Lett. A **223**, 129 (1996)